Steady-State Response of a Flexibly Mounted Stator Mechanical Face Seal Subject to Dynamic Forcing of a Flexible Rotor

Philip Varney[1]
Woodruff School of Mechanical Engineering,
Georgia Institute of Technology,
Atlanta, GA 30318
e-mail: pvarney3@gatech.edu

Itzhak Green
Professor
Woodruff School of Mechanical Engineering,
Georgia Institute of Technology,
Atlanta, GA 30318
e-mail: itzhak.green@me.gatech.edu

Mechanical face seals are constitutive components of much larger turbomachines and require consideration of the system dynamics for successful design. The dynamic interplay between the seal and rotor is intensified by recent trends toward reduced clearances, higher speeds, and more flexible rotors. Here, the "rotor" consists of the flexible shaft and the rotating seal seat. The objective here is to, for the first time, determine how the rotor affects the seal performance and vice versa. Thresholds can then be established beyond which the rotor influences the seal but not vice versa (i.e., the rotordynamics can be sent to the seal analysis as an exogenous input). To this end, a model of a flexibly mounted stator face seal is provided including the coupled dynamics of the flexible rotor. The model accounts for axial and angular deflections of the rotor and seal. Coupled rotordynamics are modeled using a lumped-parameter approach including static and dynamic rotor angular misalignments. For expediency, linearized expressions for fluid forces are used, and the resulting steady-state equations of motion are solved analytically to investigate how rotor inertia, speed, and angular misalignment influence the coupled seal dynamics. Importantly, results from the study reveal that in some operating regimes, neglecting the rotordynamics implies healthy seal operation when instead intermittent rub exists between the faces. This work also shows that when the rotor inertia is much larger than the seal inertia, the rotordynamics can be solved separately and used in the seal model as an external input. [DOI: 10.1115/1.4036380]

1 Introduction

Mechanical face seals allow rotating shafts to transfer power through fluid reservoirs of differing pressure. These seals are often delineated by noting which element, rotating or stationary, is flexibly mounted (e.g., flexibly mounted stator (FMS), flexibly mounted rotor (FMR), or flexibly mounted rotor–rotor (FMRR) seals). Mechanical face seals are also categorized according to the mechanism that produces sealing (i.e., contacting or noncontacting); this work concerns the latter, where surface separation is achieved via hydrostatic and/or hydrodynamic pressure. Noncontacting mechanical face seals are often used in applications such as nuclear reactor coolant pumps and high performance jet engines [1] because they reduce frictional losses and provide an improvement in component life. Increases in turbomachine efficiency are often achieved by reducing fluid clearances [2], increasing rotor shaft speeds, and implementing lighter and more flexible rotors.

Mechanical face seal dynamic models should improve commensurately with these heightened requirements by better accounting for rotor–seal coupling. Green and Etsion [3] provide stiffness and damping coefficients for a FMS seal, and later use these expressions to simulate the steady-state seal dynamics [4]. Similar analyses have also been performed for a FMR seal [5] to show that gyroscopic terms stabilize the FMR seal when the rotating seal element is thin. Other studies show that excessive seal vibration can cause detrimental face contact in mechanical seals [6,7]. Varney and Green [8] use rough surface contact to study intermittent contact in an otherwise noncontacting face seal. Etsion and Halperin [9] suggest the use of a surface-textured seal to reduce the possibility for face contact. Green [10] develops a transient model to analyze seal lift-off, and accounts for surface roughness, start-up/shut-down operation, and thermoelastic face coning. Lee and Green [11] develop a linearized transfer matrix method to couple the rotor and seal dynamics; the objective of their work is to eliminate rotordynamics as an explanation for unexpected phenomena seen in a particular seal test rig.

The dynamics of other seal configurations have also been discussed in the literature. Wileman and Green [12,13] develop the equations of motion for a FMRR seal configuration, where both seal elements are permitted to rotate. This configuration signifies the most generic face seal configuration and can be degenerated into any of the more common seal configurations. A later analysis [14] discusses performance differences between the most common face seal configurations. They restrict their analysis to the case of equal seal face inertia, which is justified since the rotating seal ring is considered to be the rotor. The model is later expanded to include lateral seal ring deflections [15], where constant synchronous shaft whirl couples the seal's angular vibration and the lateral whirl frequency [16].

Mechanical face seals are always constitutive components of a much larger turbomachine. A principal shortcoming of the aforementioned literature is a lack of analysis elaborating on coupling between the seal and the rotor. It should be emphasized that most previous seal dynamics works refer to the rotating seal element as the rotor; this convention is avoided here to remove confusion when discussing the actual rotor (i.e., the flexible shaft). The principal objective here is to determine how the rotor influences the seal dynamics, and by doing so, establish thresholds indicating the importance of seal–rotor dynamic coupling. To this end, a dynamic model of a noncontacting FMS seal is developed that includes dynamics of the coupled shaft (i.e., the rotor). A lumped-parameter rotordynamic model is used that accounts for conical

[1]Corresponding author.

Contributed by the Tribology Division of ASME for publication in the Journal of Tribology. Manuscript received May 9, 2016; final manuscript received March 25, 2017; published online June 14, 2017. Assoc. Editor: Mihai Arghir.

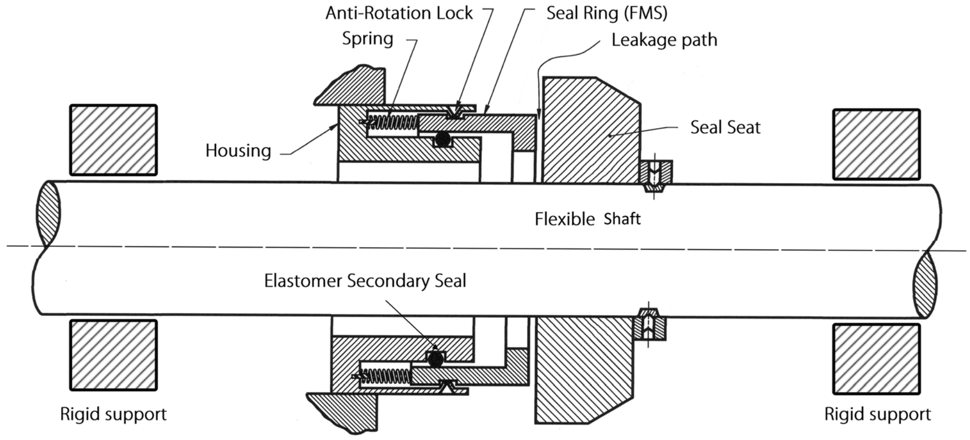

Fig. 1 FMS seal configuration showing the flexible rotor and stationary seal element

rotor vibration. The equations of motion are provided for both elements, the dynamics of which are coupled through the lubricating fluid film. For expediency, the equations of motion are rearranged to include linearized stiffness and damping coefficients, and then solved analytically to ascertain the influence of rotor-to-stator inertia ratio, shaft speed, and dynamic angular misalignment on the seal steady-state dynamic performance. This study is a novel departure from previous works concerning flexibly mounted stator–rotor (FMSR) seals [12,14] because the rotor in an FMSR seal refers to the rotating ring designed specifically to be part of the sealing apparatus. Here, the rotor consists of the flexible shaft and seal seat.

2 Modeling the Coupled Rotor-Flexibly Mounted Rotor System

The FMS mechanical face seal with an accompanying rotor is shown in Fig. 1. The stationary seal ring (i.e., the FMS) is a thin annular ring mounted to the housing using an axial support spring and a secondary seal O-ring. Rotation of the stationary element about the shaft axis is constrained by an antirotation lock. Opposite the seal ring is the flat-faced seal seat, which in this work is the rotating element (i.e., the rotor). The rotor in this case is flexibly mounted because the shaft is assumed to be flexible. A thin fluid film separates the seal faces, creating a fluid-filled region between the elements which is referred to here as the sealing dam. Face coning and relative angular tilts induce significant fluid pressure within the sealing dam; a good seal design uses this pressure to generate clearance sufficient for avoiding undesirable face contact.

In reality, most mechanical face seals are manufactured with flat faces. During lift-off and subsequent steady operation, friction and viscosity result in thermoelastic deformations which warp the seal faces and create a finite radial coning. This coning typically reaches a steady value during normal operation, which in turn results in a finite centerline clearance C_o between the seal faces. Importantly, this work assumes that the coning and clearance are constant at steady operation with known operating conditions (P_i and P_o) and geometry (the inner, outer, and balance radii). The specific value of coning at steady state can be found using a more detailed thermoelastic deformation analysis, as discussed by Green [10].

2.1 Equations of Motion. Seal elements are flexibly mounted so that the seal can track the rotor even when inevitable misalignments exist in either component. The angular kinematics of the FMS and rotor are shown in Fig. 2 using the convention of previous works [12,13,17] concerning various seal configurations (FMS, FMRR, etc.). Lateral deflections are not considered in this work. A short description of each reference frame will be useful for understanding the subsequent dynamic analyses:

(1) $\xi_s\eta_s\zeta_s$: An inertial reference frame fixed to the FMS center, O_s.
(2) $X_sY_sZ_s$: This frame is precessed about ζ_s by the precession ψ_s. X_s is the diametral line about which the FMS tilts.
(3) $x_sy_sz_s$: This FMS-principal frame is nutated about X_s by γ_s.
(4) $\xi_r\eta_r\zeta_r$: An inertial reference frame fixed to the rotor center, O_r, where ζ_r defines the axis of shaft rotation.
(5) $X_r'Y_r'Z_r'$: This frame is precessed about ζ_r by the shaft rotation angle $\alpha(t)$. If the shaft speed ω_r is constant, then $\alpha = \omega_r t$.
(6) $X_rY_rZ_r$: This frame is precessed about ζ_r by the absolute rotor precession ψ_r, or alternatively, precessed about Z_r' by the relative rotor precession ψ' (i.e., $\psi_r = \alpha(t) + \psi'$).
(7) $x_ry_rz_r$: This frame is nutated about X_r by γ_r, where X_r is selected arbitrarily with no loss of generality. The rotor spin ϕ then occurs about axis z_r.
(8) $x_r^py_r^pz_r^p$: This frame (not shown for brevity) is obtained by first applying the rotor spin ϕ about z_r and then rotating this new set of axes so that the rotor's principal moments of inertia are defined within the frame. The dynamic angular misalignment χ defines the angle between the body-fixed spinning reference frame and the principal frame.

The rotor spin ϕ has been rigorously defined in previous works (e.g., Ref. [17]). In general, the relationship between the rotor rotation angle $\alpha(t)$ and the shaft speed ω_r is given by

$$\alpha(t) = \int_0^t \omega_r(t)dt \tag{1}$$

This work assumes with no loss of generality that both inertial reference frames remain parallel, where the frames are only

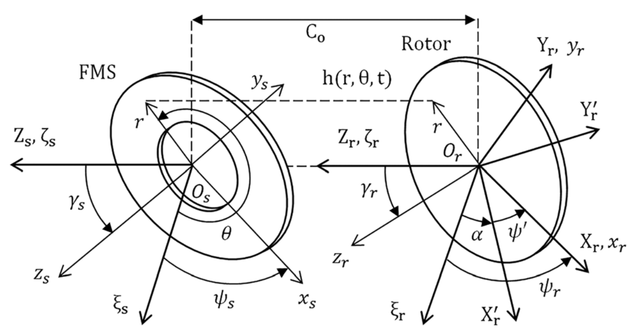

Fig. 2 Reference frames used to model the kinematics of a flexibly mounted stator mechanical face seal

translated from one another by the clearance C_o. The equations of motion are found by balancing the applied and dynamic forces and moments, using a procedure analogous to that of Wileman and Green [13]. The equations of motion for the FMS accounting for angular and axial deflections are [4,13]

$$I_{ts}\ddot{\gamma}_{\xi s} + D_s\dot{\gamma}_{\xi s} + K_s\gamma_{\xi s} = K_s\gamma_{si} + (M_f)_\xi \quad (2)$$

$$I_{ts}\ddot{\gamma}_{\eta s} + D_s\dot{\gamma}_{\eta s} + K_s\gamma_{\eta s} = (M_f)_\eta \quad (3)$$

$$m_s\ddot{u}_{zs} + D_{zs}\dot{u}_{zs} + K_{zs}u_{zs} = F_f - F_{\text{cls}} \quad (4)$$

The fluid moment about axis j is denoted $(M_f)_j$, whereas the net axial fluid force is F_f. The closing force F_{cls} on the FMS is generated by the axial support spring and fluid pressure, and will be provided in Sec. 2.3. As will be seen, these forces and moments nonlinearly depend on the seal and rotor positions (i.e., axial and angular degrees-of-freedom). The fluid film forces act on both elements, thus intrinsically coupling their motion. Any existing rotordynamic model can be used, provided that the model accounts for angular and axial deflections. For simplicity, and to establish basic principles, this work assumes the following lumped parameter rotor model:

$$\begin{aligned} I_{tr}\ddot{\gamma}_{\xi r} + I_{pr}\omega_r\dot{\gamma}_{\eta r} + D_r\dot{\gamma}_{\xi r} + K_r\gamma_{\xi r} + \omega_r D_{r\omega}\gamma_{\eta r} = -(M_f)_\xi \\ +(I_{tr} - I_{pr})\,\chi\{\omega_r^2\cos\alpha + \dot{\omega}_r\sin\alpha\} + K_r\chi_s\cos\alpha \end{aligned} \quad (5)$$

$$\begin{aligned} I_{tr}\ddot{\gamma}_{\eta r} - I_{pr}\omega_r\dot{\gamma}_{\xi r} + D_r\dot{\gamma}_{\eta r} + K_r\gamma_{\eta r} - \omega_r D_{r\omega}\gamma_{\xi r} = -(M_f)_\eta \\ +(I_{tr} - I_{pr})\,\chi\{\omega_r^2\sin\alpha - \dot{\omega}_r\cos\alpha\} + K_r\chi_s\sin\alpha \end{aligned} \quad (6)$$

$$m_r\ddot{u}_{zr} + D_{zr}\dot{u}_{zr} + K_{zr}u_{zr} = -F_f \quad (7)$$

This rotordynamic model mathematically resembles the rotating seal ring dynamics in an FMSR configuration. This resemblance is not required, and it should be emphasized once again that any suitable rotordynamic can be used in place of Eqs. (5)–(7). Because of the similarity, though, the left-hand side terms in Eqs. (5)–(7) are analogous to those derived by Wileman and Green [13]. The moments induced by dynamic angular misalignment are derived in Appendix A. The polar and transverse mass moments of inertia of element i are I_{pi} and I_{ti}, respectively (where i can be either r or s, for rotor and stator).

The stiffness and damping coefficients of the FMS are K_s and D_s for the angular modes and K_{zs} and D_{zs} for the axial modes, and are provided by Green and Etsion [18] for a seal supported by an elastomeric O-ring. In reality, the O-ring support is viscoelastic; however, in a liquid-lubricated seal, the O-ring stiffness and damping is significantly overwhelmed by that of the fluid film. In a gas-lubricated seal, an improved model for the O-ring support could be utilized by following the approach of Green and Etsion [18]. The rotor angular stiffness is K_r, which is found directly via an analysis of the rotor dimensions and material properties. External viscous damping on the rotor is described via the damping coefficient D_r, while the rotating damping coefficient is denoted $D_{\omega r}$ and is obtained by the process described by Green and Casey [19] and Varney and Green [20].

The rotor's angular misalignment manifests in two fundamentally different forms. Dynamic misalignment occurs when the rotor's principal axes of inertia do not align with the nutated referenced frame $x_r y_r z_r$; the angle between these frames is denoted χ, as discussed in Appendix A. Importantly, the angle χ references the rotor's principal moments of inertia. The second effect, static misalignment, is caused by unavoidable imperfections such as improper installation, rotor bow, and run-out, and persists even when $\omega_r = 0$. This static misalignment is an actual physical rotation with magnitude χ_s. The static rotor misalignment is imposed by applying a moment to the rotor that generates χ_s [4]. The static FMS misalignment γ_{si} occurs about ξ_s with no loss of generality.

The inertial component tilts of element i are $\gamma_{\xi i}$ and $\gamma_{\eta i}$ and are found by solving the equations of motion. These components comprise each element's total tilt $\gamma_i^2 = \gamma_{\xi i}^2 + \gamma_{\eta i}^2$ and precession $\tan\psi_i = \gamma_{\eta i}/\gamma_{\xi i}$. The seal's performance is neatly summarized by calculating the relative tilt γ^* between the elements [21]

$$(\gamma^*)^2 = \gamma_s^2 + \gamma_r^2 - 2\gamma_s\gamma_r\cos(\psi_s - \psi_r) \quad (8)$$

Successful seal operation is characterized by small relative misalignments, since the objective of the flexible mount is to allow one element to track the other. Since the seal considered here is designed so that $P_o > P_i$, the film thickness contribution from face coning is minimum at the inner radius r_i. Taking this into consideration, the critical relative tilt beyond which contact occurs is $\gamma_{\text{cr}}^* = C/r_i$ [3], where C is the centerline clearance between the seal ring and rotor.

2.2 Film Thickness Between the Flexibly Mounted Stator and Rotor. Since lateral deflections are not considered here, it will be judicious to describe any point in the sealing dam using the inertial $r\theta$ coordinate system as shown in Fig. 2. Using this coordinate system, the fluid film clearance between the seal elements is

$$\begin{aligned} h(r,\theta,t) = C_o + (u_{zs} - u_{zr}) + \gamma_s r\sin(\theta - \psi_s) \\ - \gamma_r r\sin(\theta - \psi_r) + \beta^*(r - r_i) \end{aligned} \quad (9)$$

where β^* is the magnitude of face coning. In this work, coning is assumed to be time invariant, even though in transient operation the coning is often generated by thermoelastic and centrifugal deformations [10]. Circumferential and time derivatives of the film thickness will be needed to evaluate the fluid forces and moments acting on the seal elements. These derivatives are

$$\frac{\partial h}{\partial\theta} = \gamma_s r\cos(\theta - \psi_s) - \gamma_r r\cos(\theta - \psi_r) \quad (10)$$

$$\begin{aligned} \frac{\partial h}{\partial t} = \dot{u}_{zs} - \dot{u}_{zr} + \dot{\gamma}_s r\sin(\theta - \psi_s) - \dot{\psi}_s\gamma_s r\cos(\theta - \psi_s) \\ - \dot{\gamma}_r r\sin(\theta - \psi_r) + \dot{\psi}_r\gamma_r r\cos(\theta - \psi_r) \end{aligned} \quad (11)$$

2.3 Fluid Film Forces and Moments. The fluid film pressures depend on the clearance C_o, which itself depends on the coning angle and balance radii (in addition to the known operating conditions). Here, a clearance and coning angle are selected a priori; balancing the opening and closing forces on the flexibly mounted element then provides the balance radius r_b which enforces the selected clearance. The opening force is generated solely by fluid pressure within the sealing dam, while the closing force arises from the radially mounted spring and fluid forces acting on the backside of the seal ring. The static pressure profile is solved from the Reynolds equation using the narrow seal approximation [22]

$$P_s(r,\theta) = P_o - (P_o - P_i)\frac{h_i^2}{h_o^2 - h_i^2}\left[\left(\frac{h_o}{h}\right)^2 - 1\right] \quad (12)$$

where the subscripts "o" and "i" represent outer and inner parameters, respectively. Integrating this axisymmetric static pressure profile across the sealing dam gives the fluid film opening force. The closing force is found by summing the spring and pressure forces acting on the seal ring backside

$$F_{\text{cls}} = F_{\text{spr}} + \pi[P_o(r_o^2 - r_b^2) + P_i(r_b^2 - r_i^2)] \quad (13)$$

In this work, the spring force is assumed to be constant ($F_{\text{spr}} \neq F_{\text{spr}}(u_z)$) since the axial deflections are small. These equations are then used to select a balance radius r_b yielding the clearance C_o.

Angular tilts and shaft rotation result in hydrodynamic fluid forces. The hydrodynamic pressure is found by analytically solving the isoviscous and incompressible Reynolds equation using the narrow seal approximation [23–25]

$$P_d(r,\theta,t) = -3\mu\left(\omega_r\frac{\partial h}{\partial\theta}+2\frac{\partial h}{\partial t}\right)\frac{(r_o-r)(r-r_i)}{h_m h^2} \tag{14}$$

where $h_m = h(r_m,\theta)$, r_m is the mean seal ring radius, and μ is the fluid viscosity. For the parameters given in Table 1, the narrow seal approximation results in less than 2% error in the fluid film force calculations [23]. The total fluid pressure $P_f(r,\theta,t)$ is the sum of the hydrostatic (Eq. (12)) and hydrodynamic (Eq. (14)) components

$$P_f(r,\theta,t) = \max[P_s(r,\theta,t)+P_d(r,\theta,t),0] \tag{15}$$

where the conditional statement applies the half-Sommerfeld boundary condition to account for the possibility of cavitation. The fluid film moments and axial force are found by integrating the pressure over the sealing dam

$$M_\xi = \int_0^{2\pi}\int_{r_i}^{r_o} P_f(r,\theta,t)r^2\sin\theta\,dr\,d\theta \tag{16}$$

$$M_\eta = -\int_0^{2\pi}\int_{r_i}^{r_o} P_f(r,\theta,t)r^2\cos\theta\,dr\,d\theta \tag{17}$$

$$F_z = \int_0^{2\pi}\int_{r_i}^{r_o} P_f(r,\theta,t)r\,dr\,d\theta \tag{18}$$

These integrals can be evaluated at any instant in time by discretizing the sealing dam and applying a suitable numeric integration scheme (e.g., Simpson's rule or Gaussian quadrature).

2.4 Linearized Equations of Motion. The equations of motion (Eqs. (2)–(7)) require multiple integrations of the fluid pressure at each time step in the solution process; this numeric approach is tedious and inhibits a comprehensive investigation of seal performance. Several realistic assumptions can be applied to reduce the fluid film to associated stiffness and damping coefficients. The first of these assumptions is that the seal ring is narrow, which is typically true for most practical face seals. The second assumption is that the seal experiences only small deflections (angular and axial) about a steady operational state. This assumption is reasonable for this work since (a) the seal is balanced a priori, and (b) only parameters' regimes which avoid face contact are considered. The final assumption is that the hydrostatic pressure generated in the sealing dam is sufficient to suppress cavitation.

The fluid film stiffness and damping coefficients, K_f and D_f, are found analytically by Wileman and Green [12] for the general case of a FMRR configuration in which both seal elements are permitted to rotate (this work omits the laborious mathematics for brevity). These coefficients are applicable here since the FMS-flexible rotor configuration is a degenerate case of the FMRR configuration. An important conclusion from their work is that linearizing about a stable operating mode decouples the angular and axial degrees-of-freedom. Since shaft axial stiffness is typically large, and the FMS is assumed to be balanced, the axial linearized equations of motion will not be considered herein.

The linearized fluid film stiffness and damping coefficients are

$$K_f = \pi(P_o-P_i)(\beta R_i-1)E_o^2\frac{r_o^4}{C_o} \tag{19}$$

$$D_f = 2\pi R_m^3 G_o\frac{S r_o^4}{C_o\omega_r} \tag{20}$$

where

$$S = 6\mu\omega_r\left(\frac{r_o}{C_o}\right)^2\left(1-R_i^2\right) \tag{21}$$

$$E_o = \frac{(1-R_i)R_m}{2+\beta(1-R_i)} \tag{22}$$

$$G_o = \frac{\ln(1+\beta(1-R_i)) - \dfrac{2\beta(1-R_i)}{2+\beta^*(1-R_i)}}{\beta^3(1-R_i)^2} \tag{23}$$

Normalized terms in the above expressions are given by $R = r/r_o$ and $\beta = \beta^* r_o/C_o$. These fluid film coefficients are then used to express the fluid forces and moments [12]. The steady-state linearized equations of motion for angular tilts of both elements, including K_f and D_f, are then

$$\begin{aligned} &I_{ts}\ddot{\gamma}_{\xi s} + (D_s+D_f)\dot{\gamma}_{\xi s} - D_f\dot{\gamma}_{\xi r} + (K_s+K_f)\gamma_{\xi s} \\ &\quad - K_f\gamma_{\xi r} + \frac{1}{2}\omega_r D_f(\gamma_{\eta s}-\gamma_{\eta r}) = K_s\gamma_{si} \end{aligned} \tag{24}$$

$$\begin{aligned} &I_{ts}\ddot{\gamma}_{\eta s} + (D_s+D_f)\dot{\gamma}_{\eta s} - D_f\dot{\gamma}_{\eta r} + (K_s+K_f)\gamma_{\eta s} \\ &\quad - K_f\gamma_{\eta r} + \frac{1}{2}\omega_r D_f(\gamma_{\xi r}-\gamma_{\xi s}) = 0 \end{aligned} \tag{25}$$

$$\begin{aligned} &I_{tr}\ddot{\gamma}_{\xi r} + I_{pr}\omega_r\dot{\gamma}_{\eta r} + (D_r+D_f)\dot{\gamma}_{\xi r} - D_f\dot{\gamma}_{\xi s} + (K_r+K_f)\gamma_{\xi r} \\ &\quad - K_f\gamma_{\xi s} + \omega_r D_{r\omega}\gamma_{\eta r} + \frac{1}{2}\omega_r D_f(\gamma_{\eta r}-\gamma_{\eta s}) \\ &= \left\{(I_{tr}-I_{pr})\chi\omega_r^2 + K_r\chi_s\right\}\cos(\omega_r t) \end{aligned} \tag{26}$$

$$\begin{aligned} &I_{tr}\ddot{\gamma}_{\eta r} - I_{pr}\omega_r\dot{\gamma}_{\xi r} + (D_r+D_f)\dot{\gamma}_{\eta r} - D_f\dot{\gamma}_{\eta s} \\ &\quad + (K_r+K_f)\gamma_{\eta r} - K_f\gamma_{\eta s} - \omega_r D_{r\omega}\gamma_{\xi r} \\ &\quad + \frac{1}{2}\omega_r D_f(\gamma_{\xi s}-\gamma_{\xi r}) = \left\{(I_{tr}-I_{pr})\chi\omega_r^2 + K_r\chi_s\right\}\sin(\omega_r t) \end{aligned} \tag{27}$$

where $\alpha = \omega_r t$ since the shaft speed is constant. These equations are expressed in matrix form

$$[M]\{\ddot{q}\} + ([D]+\omega_r[G])\{\dot{q}\} + [K]\{q\} = \{F\} \tag{28}$$

where $[M]$ is the mass matrix, $[D]$ and $[G]$ contain damping and gyroscopic terms, respectively, and $[K]$ is the stiffness matrix. The state vector $\{q\}$ contains the FMS and rotor angular degrees-of-freedom, and $\{F\}$ contains all forcing functions. This set of linear ordinary differential equations is solved analytically to provide a

Table 1 Seal and lubricant properties

Parameter	
Viscosity	1.2 mPa·s
Pressure differential, $P_o - P_i$	400 kPa
Set point clearance, C_o	1 μm
Coning, β^*	1 mrad
Inner radius, r_i	0.0355 m
Outer radius, r_o	0.0408 m
Closing force, F_{cls}	20 N

Table 2 Rotor and seal dynamic and support properties

Parameter	Rotor	FMS
Polar moment of inertia	$I_{pr} = 1/\delta\, I_{tr}$ kg/m^2	—
Transverse moment of inertia	$I_{tr} = 0.2$ kg/m^2	$I_{ts} = 1.7 \times 10^{-3}$ kg/m^2
Mass	$m_r = 10$ kg	$m_s = 0.1$ kg
Angular support stiffness	$K_r = 5 \times 10^5$ N·m/rad	$K_s = 363.9$ N·m/rad
Angular external/support damping	$D_r = 20$ N·m s/rad	$D_s = 0.22$ N·m s/rad
Rotating damping	$D_{\omega r} = 1$ N·m s/rad	—

closed-form steady-state solution from which general trends in seal behavior can be expediently extracted. The angular whirl frequencies are found by setting $\{F\} = 0$ and assuming a solution $\bar{q}_0 = \bar{A}\exp(\lambda t)$. This procedure yields the characteristic equation whose roots are the system whirl frequencies. Likewise, the steady-state forced response solution is found by assuming a solution in the form $\bar{q} = \bar{C} + \bar{\Gamma}\exp(i\omega_r t)$, where $\bar{C}$ is the constant response to the static seal misalignment and $\bar{\Gamma}$ is the steady-state dynamic response to the rotor misalignment. The free and forced response solutions are provided in Appendix B.

The equations of motion for a FMSR seal configuration can be obtained from Eqs. (24)–(27) by replacing the distinct rotating damping coefficient $D_{\omega r}$ with the rotor damping coefficient D_r. However, a distinct difference exists in the mechanism by which the rotor stiffness and damping coefficients are obtained. In a FMSR seal, these coefficients are found from the flexible support, namely, the elastomeric O-ring used to attach the rotating seal ring to the primary rotor. When the shaft rotordynamics are concerned, the rotor stiffness and damping coefficients are found from the material and geometry properties of the rotor.

The linearized equations of motion and steady-state solution are not given as a panacea to be used in lieu of investigating the full nonlinear equations of motion. Rather, the linearized equations of motion are a tool that can be used to expediently extract trends in the rotor response for a wide range of possible design parameters such as misalignment, rotor inertia ratio, and shaft speed. Any analysis of a particular seal configuration should first verify that the linearized equations are valid in the considered regime of parameters.

3 Results

The objective of this study is to quantify the rotor's influence on the FMS seal dynamics; because the FMS is designed to track misalignments in the rotating element, the seal's performance will be quantified with respect to the relative tilt between the rotor and stator (Eq. (8)). The parameters used here are given in Tables 1 and 2 for the dynamic and sealing parameters, respectively. The FMS stiffness and damping values used here, K_s and D_s, are representative of values obtained from an existing experimental FMS seal test rig [7]. Likewise, the rotor parameters K_r and D_r are representative of the rotor found in an associated experimental test rig [19,20]. Parameters not specified, such as the inertia ratio $\delta = I_{tr}/I_{pr}$, dynamic angular misalignment χ, and shaft speed ω_r, will be provided wherever applicable. The static misalignments γ_{si} and χ_s are not considered here since linear superposition applies to the linearized equations of motion; the system response to these terms can be found independently and added to the response to dynamic rotor misalignment.

The efficacy of the linearized steady-state analytic solution is established by comparing the solution to that found by solving numerically the full nonlinear equations of motion (Eqs. (2)–(7)). The nonlinear equations of motion were solved numerically using MATLAB's ODE15s; the relative and absolute tolerances were obtained by progressively tightening the tolerance until convergence was obtained. The relative tilt versus shaft speed is shown in Fig. 3 for several values of dynamic angular misalignment. The relative tilt reaches a local maximum at 990 rad/s; this peak occurs identically at the rotor's first $1\times$ forward critical speed. Importantly, the appearance of the rotor's critical speed response in the relative tilt indicates that the rotordynamics have a profound influence on the seal performance for the parameters considered here.

Several observations can also be made regarding the veracity of the analytic steady-state solution. For the parameters considered here, it is clear that the analytic steady-state solution is most accurate for small misalignments and shaft speeds at or above the rotor's critical speed. These conclusions are reasonable because the linearized fluid film rotordynamic coefficients are found by assuming that the rotor deflections are small. Even though the solutions diverge in certain regimes, the analytic steady-state solution is sufficiently accurate for investigating parametric trends, and particularly so for small misalignments and shaft speeds beneath the critical speed.

Dynamic coupling between the rotor and stator is investigated by varying the ratio between the rotor and FMS transverse mass moments of inertia. The dynamic response of a thick rotor ($\delta = 2$) to an angular misalignment of $\chi = 0.5$ mrad is given in Fig. 4, which shows relative tilt γ^* versus shaft speed ω_r for several transverse inertia ratios. In addition, the dynamic response of only the rotor (i.e., no sealing apparatus) is provided for comparison. As expected, the FMS and rotor are essentially decoupled for inertia ratios I_{tr}/I_{ts} above 100. The importance of this conclusion cannot be understated, as it implies that for massive rotors ($I_{tr} \gg I_{ts}$), the rotordynamics influence the seal dynamics but not vice versa. Thus, the rotordynamics can be solved independently and sent as a known input to a separate seal dynamics model.

Significant dynamic amplification is seen for certain inertia ratios I_{tr}/I_{ts} when the rotor is thick ($I_{tr}/I_{pr} > 1$). This phenomenon is shown in Fig. 5 for both a thin and a thick rotor by observing the maximum relative tilt γ^* versus inertia ratio I_{tr}/I_{ts}. The relative tilt versus shaft speed profile is found for each inertia ratio (see Fig. 4, for example, profiles) from which the maximum

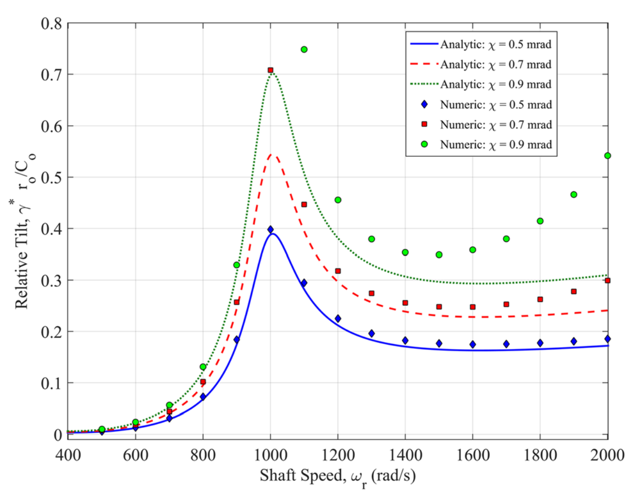

Fig. 3 Comparing the numeric solution of the full nonlinear equations of motion to the analytic solution of the linearized equations of motion ($\delta = 2$)

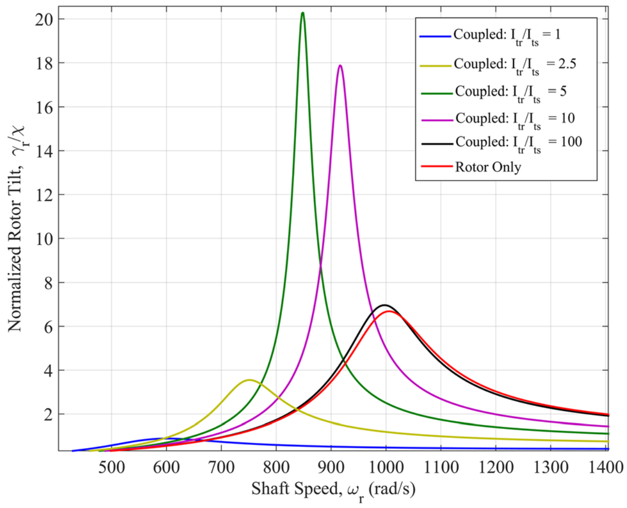

Fig. 4 Investigating the influence of FMS dynamics on rotor response for an angular misalignment of $\chi = 0.5$ mrad, $\delta = 2$

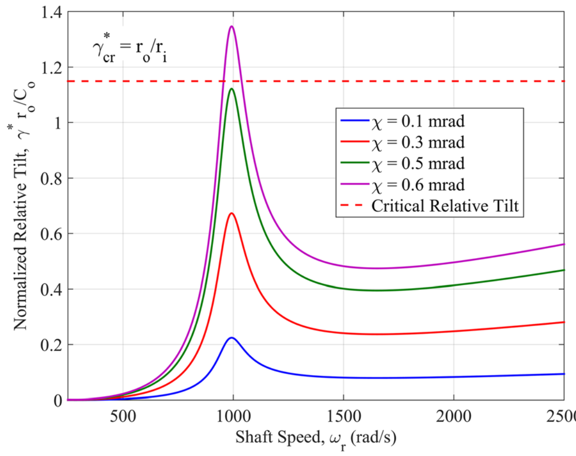

Fig. 6 Relative tilt versus shaft speed for several values of angular misalignment, highlighting the appearance of face contact when coupled rotordynamics are included ($\delta = 2$, $I_{tr}/I_{ts} = 50$)

relative tilt is recorded. For a thin rotor, the relative tilt decreases monotonically as the inertia ratio increases (Fig. 5(*b*)). On the other hand, Fig. 5(*a*) indicates that the relative tilt for a thick rotor reaches its maximum value when $I_{tr}/I_{ts} = 6.48$ and $\omega_r = 877.3$ rad/s (this occurs at maximum when the system characteristic equation is minimized).

Seal face contact occurs when the relative tilt exceeds the maximum allowable clearance. In an outward-pressurized seal with the inward flow, first contact occurs along the inner radius, at a

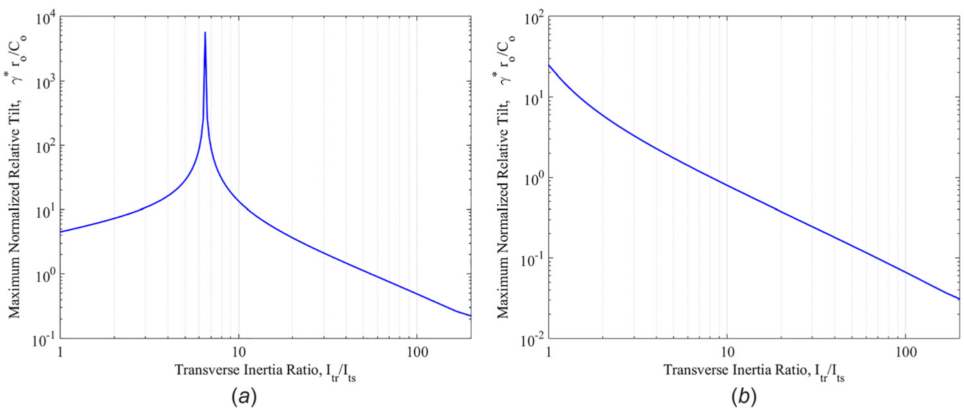

Fig. 5 Relative tilt versus rotor–stator inertia ratio for thin and thick rotors: (*a*) thick rotor ($\delta = 2$) and (*b*) thin rotor ($\delta = 0.5$)

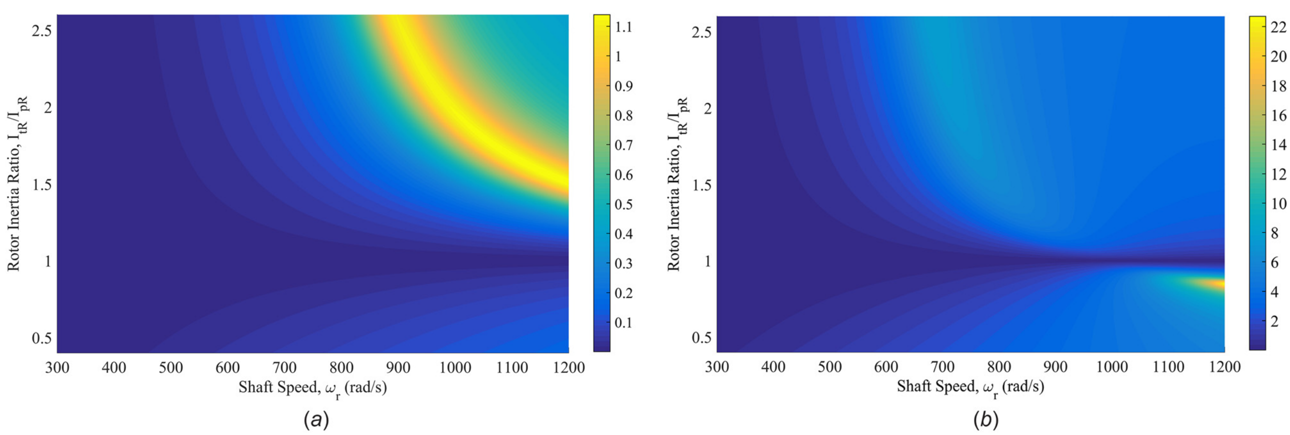

Fig. 7 Relative tilt versus shaft speed ω_r and rotor inertia ratio $\delta = I_{tr}/I_{pr}$ ($\chi = 0.5$ mrad): (*a*) case when the rotor inertia is much larger than the FMS ($I_{tr}/I_{ts} = 50$) and (*b*) case when the rotor inertia is comparable to the FMS ($I_{tr}/I_{ts} = 2$)

critical value of $\gamma^*_{\rm cr} = C_o/r_i$; any relative tilt exceeding this value precipitates face contact. A dangerous ramification of neglecting the rotordynamics is that the analysis may predict healthy operation when face contact occurs. This result is shown in Fig. 6 for a thick rotor, where the rotor tilt is provided versus shaft speed for several values of rotor angular misalignment. Clearly, operating near the rotor's critical speed of 990 rad/s results in the onset of contact.

One solution for minimizing the effect of coupled rotordynamics is to ensure that the rotor is thin. In this case, gyroscopic effects stabilize the rotor and eliminate the forward critical speed of the rotor [26]. Figure 7 gives the normalized relative tilt $\gamma^* r_o/C_o$ versus shaft speed and rotor inertia ratio I_{tr}/I_{pr}. When the rotor inertia is much larger than that of the stator (Fig. 7(*a*)), no critical speed response is observed when the rotor is thin. On the other hand, the dynamics of a system where the rotor and the stator inertia are comparable are more complicated (Fig. 7(*b*)), and no general conclusions can be made regarding rotor inertia ratio.

4 Conclusions

The importance of studying the effect of shaft rotordynamics on FMS seal performance increases as shafts are made lighter and more flexible and clearances are reduced. The full nonlinear equations of motion for a FMS seal coupled to the angular dynamics of a flexible rotor have been presented, where the two elements are coupled via forces and moments generated via a thin fluid film between the faces. The equations of motion are linearized using existing stiffness and damping coefficients and solved exactly to provide a closed-form solution for the system's steady-state response to angular misalignment. The linearized steady-state solution is shown to be most precise for small misalignments and shaft speeds beneath the critical speed, though the results in all cases are qualitatively similar for the parameters considered here. For this reason, the linearized steady-state solution is used to expediently extract trends in the system performance for a wide range of parameters.

The relative tilt between the faces is strongly influenced by the rotordynamics and displays significant amplification near the synchronous rotor critical speeds. The results presented herein indicate that an analysis which fails to consider the rotordynamics may incorrectly predict healthy seal operation, when in reality the rotordynamics precipitate face contact. For thick rotors, significant dynamic amplification is seen when the inertia of the rotor and FMS seal are comparable in magnitude. When the rotor inertia increases significantly beyond that of the stator, the seal dynamics no longer influence those of the rotor, and the rotordynamics can then be solved separately and sent as an input to the seal model equations. For a system where the rotor inertia is much larger than the FMS seal inertia, the designer is encouraged to ensure that a thin rotor is used, since gyroscopic effects stabilize the system and eliminate resonance at the critical speed.

Investigating the influence of rotordynamics on seal performance has ramifications beyond seal design. Since the elements are intrinsically coupled via the fluid film, any shaft rotordynamic vibration signatures are also transferred to the FMS seal. In such a manner, a mechanical face seal could perhaps be used as a cost-effective surrogate for rotordynamic vibration monitoring.

Nomenclature

C_o = set-point centerline clearance
D_f = fluid film angular damping coefficient
D_r = rotor angular external damping coefficient
D_s = FMS support angular damping coefficient
D_{sz} = axial support damping coefficient
$D_{\omega r}$ = rotor angular rotating damping coefficient
$F_{\rm cls}$ = closing force
$F_{\rm spr}$ = radial spring force
$h(r, \theta, t)$ = sealing dam film thickness
I_{pi} = polar mass moment of inertia of element i
I_{ti} = transverse mass moment of inertia of element i
K_f = fluid film angular stiffness coefficient
K_s = angular support stiffness coefficient
K_{zs} = axial support stiffness coefficient
m_r = rotor mass
m_s = flexibly mounted stator mass
P_i = inner fluid pressure
P_o = outer fluid pressure
r_b = seal ring balance radius
r_i = inner seal ring radius
r_m = mean seal ring radius
r_o = outer seal ring radius
$r\theta$ = inertial polar coordinate system
u_{zi} = axial deflection of element i
α = shaft rotation angle
β = nondimensional FMS coning angle
β^* = dimensional FMS coning angle
γ_r = magnitude of rotor tilt
γ_s = magnitude of FMS tilt
γ_{si} = static FMS misalignment tilt
$\gamma_{\eta i}$ = angular tilt about η for element i
$\gamma_{\xi i}$ = angular tilt about ξ for element i
δ = rotor inertia ratio, I_{tr}/I_{pr}
Δ = characteristic equation of the system
μ = fluid viscosity
ϕ = rotor spin rate
χ = dynamic rotor angular misalignment
χ_s = static rotor angular misalignment
ψ_r = rotor precession
ψ_s = stator precession
ω_r = shaft rotation rate

Appendix A: Deriving the Dynamic Misalignment Forcing Function

A dynamic moment is generated on the rotor when the principal axes $x_r^p y_r^p z_r^p$ do not align with the spin axes $1_r 2_r 3_r$. The rotor spin ϕ occurs within the nutated reference frame $x_r y_r z_r$, which are shown in Fig. 2 and discussed in detail in Sec. 2.1. The kinematic constraint between the rotor precession and spin [17,27] is $\phi = \alpha(t) - \psi_r$, and will be useful for deriving the dynamic misalignment moments.

The rotation matrix that transforms the nutated frame $x_r y_r z_r$ to the spin frame $1_r 2_r 3_r$ is denoted $[R_{z_r}(\phi)]$, signifying that the magnitude of the rotation is ϕ and occurs about the z_r axis. The principal frame is rotated from the body-fixed spin frame by the angle χ, which is assumed to occur about axis 1_r without any loss of generality. The relevant rotation matrix that moves a vector between the spin axes and the principal axes is $[R_{1_r}(\chi)]$. The total rotation matrix $[R]$ moving a vector between $x_r y_r z_r$ and $x_r^p y_r^p z_r^p$ is therefore

$$[R] = [R_{1_r}(\chi)][R_{z_r}(\phi)] = \begin{bmatrix} 1 & 0 & 0 \\ 0 & \cos\chi & \sin\chi \\ 0 & -\sin\chi & \cos\chi \end{bmatrix} \begin{bmatrix} \cos\phi & \sin\phi & 0 \\ -\sin\phi & \cos\phi & 0 \\ 0 & 0 & 1 \end{bmatrix} \tag{A1}$$

which for small misalignments $\chi \ll 1$ becomes

$$[R] = \begin{bmatrix} \cos\phi & \sin\phi & 0 \\ -\sin\phi & \cos\phi & \chi \\ \chi\sin\phi & -\chi\cos\phi & 1 \end{bmatrix} \tag{A2}$$

The principal inertia tensor $[I]$ for the rotor is transformed into the nutated reference frame $x_r y_r z_r$ by the following expression:

$$[I]_{x_r y_r x_r} = [R]^{\mathrm{T}} \begin{bmatrix} I_{tr} & 0 & 0 \\ 0 & I_{tr} & 0 \\ 0 & 0 & I_{pr} \end{bmatrix} [R] = \begin{bmatrix} I_{tr} + (I_{pr} - I_{tr})\chi^2 \sin^2\phi & -\frac{1}{2}\chi^2 (I_{pr} - I_{tr})\sin 2\phi & (I_{pr} - I_{tr})\chi \sin\phi \\ -\frac{1}{2}\chi^2 (I_{pr} - I_{tr})\sin 2\phi & I_{tr} & -(I_{pr} - I_{tr})\chi \cos\phi \\ (I_{pr} - I_{tr})\chi \sin\phi & -(I_{pr} - I_{tr})\chi \cos\phi & I_{pr} \end{bmatrix} \quad \text{(A3)}$$

For small misalignments, this result reduces to the following, where the subscripts on the inertia tensor are dropped henceforth for brevity:

$$[I] = \begin{bmatrix} I_{tr} & 0 & (I_{pr} - I_{tr})\chi \sin\phi \\ 0 & I_{tr} & -(I_{pr} - I_{tr})\chi \cos\phi \\ (I_{pr} - I_{tr})\chi \sin\phi & -(I_{pr} - I_{tr})\chi \cos\phi & I_{pr} \end{bmatrix} \quad \text{(A4)}$$

This inertia tensor is now time dependent, since the spin angle ϕ depends on the rotor precession and the shaft rotation rate. The dynamic moments for the rotor, assuming that the center of the rotor O_r is the center of mass, are [26]

$$\bar{M}_{O_r} = \frac{\partial(\bar{h}_{O_r})}{\partial t} + \Omega_{x_r y_r z_r} \times (\bar{h}_{O_r}) \quad \text{(A5)}$$

The angular velocity of the reference frame $x_r y_r z_r$ is provided in previous works [12,26]. The rotor's angular momentum is $\bar{h}_{O_r} = [I]\bar{\lambda}$, where in this context $\bar{\lambda}$ is the absolute angular velocity of the rotor [17]. The time-dependent inertia matrix manifests primarily in the first term in Eq. (A5)

$$\frac{\partial(\bar{h}_{O_r})}{\partial t} = \frac{\partial[I]}{\partial t}\bar{\lambda} + [I]\frac{\partial\bar{\lambda}}{\partial t} \quad \text{(A6)}$$

Evaluating Eq. (A5) using the time-dependent inertia matrix is laborious, and the details are omitted here for brevity. Once the dynamic moments are found, they are transformed from the nutating reference frame into the inertial reference frame (see Sec. 2.1 for details on the intermediate frames)

$$\begin{aligned} (\bar{M}_{O_r})_{\xi_r \eta_r \zeta_r} &= [R_{Z_r}(\psi_r)]^{\mathrm{T}} [R_{x_r}(\gamma_r)]^{\mathrm{T}} (\bar{M}_{O_r})_{x_r y_r z_r} \\ &= \begin{Bmatrix} I_{tr}\ddot{\gamma}_{\xi r} + I_{pr}\omega_r \dot{\gamma}_{\eta r} + (I_{pr} - I_{tr})\chi(\omega_r^2 \cos\alpha + \dot{\omega}_r \sin\alpha) \\ I_{tr}\ddot{\gamma}_{\eta r} - I_{pr}\omega_r \dot{\gamma}_{\xi r} + (I_{pr} - I_{tr})\chi(\omega_r^2 \sin\alpha - \dot{\omega}_r \cos\alpha) \\ O(\gamma_r^2) \end{Bmatrix} \end{aligned} \quad \text{(A7)}$$

where the rotation matrices obey the labeling convention established earlier.

Appendix B: Free and Forced Response Solutions

B.1 Free Response

The system's whirl frequencies λ are found from the linearized equations of motion, Eqs. (24)–(27), by setting the forcing terms equal to zero and inserting a solution $\bar{q}_0 = \bar{A}\exp(\lambda t)$. This procedure yields the characteristic equation whose roots are the generally nonsynchronous whirl frequencies

$$p(\lambda, \omega_r) = p_4\lambda^4 + p_3\lambda + p_2\lambda + p_1\lambda + p_0 = 0 \quad \text{(B1)}$$

where

$$\begin{aligned} p_4 &= I_{ts} I_{tr} \\ p_3 &= -i(D_2 I_{ts} + D_1 I_{tr} - i I_{pr} I_{ts}\omega_r) \\ p_2 &= i\omega_r\left(D_1 I_{pr} + \frac{1}{2}D_f(I_{tr} + I_{ts}) + D_{\omega r} I_{ts}\right) \\ &\quad + D_f^2 - D_1 D_2 - I_{tr}K_1 - I_{ts}K_2 \\ p_1 &= -\frac{1}{2}iD_f I_{pr}\omega_r^2 + \left(\frac{1}{2}(D_1 + D_2)D_f - D_f^2\right. \\ &\quad \left. + D_1 D_{\omega r} + I_{pr}K_1\right)\omega_r + i(D_1 K_2 + D_2 K_1 - 2D_f K_f) \\ p_0 &= K_1 K_2 - K_f^2 - \frac{1}{2}D_f D_{\omega r}\omega_r^2 \\ &\quad - \frac{1}{2}i\omega_r(D_f K_2 - 2D_f K_f + 2D_{\omega r}K_1 + D_f K_1) \end{aligned} \quad \text{(B2)}$$

where $D_1 = D_s + D_f$, $D_2 = D_r + D_f$, $K_1 = K_s + K_f$, and $K_2 = K_r + K_f$.

B.2 Forced Response

The linearized equations of motion, Eqs. (25)–(28), are solved exactly to provide the steady-state solution to static and dynamic misalignment. Assuming a solution $\bar{q} = \bar{\Gamma}\exp(i\omega_r t)$ and inserting into Eqs. (24)–(27) gives the following steady-state solution:

$$\bar{\Gamma} = \frac{1}{\Delta}\left\{(I_{tr} - I_{pr})\chi\omega_r^2 + K_r\chi_s\right\} \begin{Bmatrix} 2iK_f - D_f\omega_r \\ 2K_f + iD_f\omega_r \\ 2i(K_f + K_s - I_{ts}\omega_r^2) - \omega_r(D_f + 2D_s) \\ 2(K_f + K_s - I_{ts}\omega_r^2) + i\omega_r(D_f + 2D_s) \end{Bmatrix} \quad \text{(B3)}$$

where Δ is

$$\Delta = S_4\omega_r^4 + S_3\omega_r^3 + S_2\omega_r^2 + S_1\omega_r + S_0 \quad \text{(B4)}$$

and

$$\begin{aligned} S_4 &= 2iI_{ts}(I_{pr} - I_{tr}) \\ S_3 &= (D_f + 2D_s)(I_{pr} - I_{tr}) + (2D_{\omega r} - D_f - 2D_r)I_{ts} \\ S_2 &= i\left[(D_f + 2D_s)(D_r - D_{\omega r}) + D_f D_s\right. \\ &\quad \left. + 2(K_f + K_s)(I_{tr} - I_{pr}) + 2I_{ts}(K_f + K_r)\right] \\ S_1 &= (D_f + 2D_s)K_r + 2(D_r + D_s + D_{\omega r})K_f \\ &\quad + (D_f + 2D_r - 2D_{\omega r})K_s S_0 = -2i(K_f K_r + K_f K_s + K_r K_s) \end{aligned} \quad \text{(B5)}$$

References

[1] Steinetz, B. M., Hendricks, R. C., and Munson, J., 1998, "Advanced Seal Technology Role in Meeting Next Generation Turbine Engine Goals," NASA, Lewis Research Center, Cleveland, OH, Technical Report No. 20000020798.

[2] Chupp, R. E., Hendricks, R. C., Lattime, S. B., and Steinetz, B. M., 2006, "Sealing in Turbomachinery," NASA, Glenn Research Center, Cleveland, OH, Technical Report No. 2006-214341.

[3] Green, I., and Etsion, I., 1983, "Fluid Film Dynamic Coefficients in Mechanical Face Seals," ASME J. Lubr. Technol., **105**(2), pp. 297–302.
[4] Green, I., and Etsion, I., 1986, "Nonlinear Dynamic Analysis of Noncontacting Coned-Face Mechanical Seals," ASLE Trans., **29**(3), pp. 383–393.
[5] Green, I., 1990, "Gyroscopic and Damping Effects on the Stability of a Noncontacting Flexibly-Mounted Rotor Mechanical Face Seal," *Dynamics of Rotating Machinery*, Hemisphere, Carlsbad, CA, pp. 153–157.
[6] Etsion, I., and Constantinescu, I., 1984, "Experimental Observation of the Dynamic Behavior of Noncontacting Coned-Face Mechanical Seals," ASLE Trans., **27**(3), pp. 263–270.
[7] Lee, A. S., and Green, I., 1995, "An Experimental Investigation of the Steady-State Response of a Noncontacting Flexibly Mounted Rotor Mechanical Face Seal," ASME J. Tribol., **117**(1), pp. 153–159.
[8] Varney, P., and Green, I., 2016, "Impact Phenomena in a Non Contacting Mechanical Face Seal," ASME J. Tribol., **139**(2), p. 022201.
[9] Etsion, I., and Halperin, G., 2002, "A Laser Surface Textured Hydrostatic Mechanical Seal," Tribol. Trans., **45**(3), pp. 430–434.
[10] Green, I., 2002, "A Transient Dynamic Analysis of Mechanical Seals Including Asperity Contact and Face Deformation," Tribol. Trans., **45**(3), pp. 284–293.
[11] Lee, A. S., and Green, I., 1994, "Rotordynamics of a Mechanical Face Seal Riding on a Flexible Shaft," ASME J. Tribol., **116**(2), pp. 345–351.
[12] Wileman, J., and Green, I., 1991, "The Rotordynamic Coefficients of Mechanical Seals Having Two Flexibly Mounted Rotors," ASME J. Tribol., **113**(4), pp. 795–804.
[13] Wileman, J., and Green, I., 1997, "Steady-State Analysis of Mechanical Seals With Two Flexibly Mounted Rotors," ASME J. Tribol., **119**(1), pp. 200–204.
[14] Wileman, J., and Green, I., 1999, "Parametric Investigation of the Steady-State Response of a Mechanical Seal With Two Flexibly Mounted Rotors," ASME J. Tribol., **121**(1), pp. 69–76.
[15] Wileman, J., and Green, I., 1996, "The Rotor Dynamic Coefficients of Eccentric Mechanical Face Seals," ASME J. Tribol., **118**(1), pp. 215–224.
[16] Wileman, J., 2004, "Dynamic Response of Eccentric Face Seals to Synchronous Shaft Whirl," ASME J. Tribol., **126**(2), pp. 301–309.
[17] Green, I., 2008, "On the Kinematics and Kinetics of Mechanical Seals, Rotors, and Wobbling Bodies," Mech. Mach. Theory, **43**(7), pp. 909–917.
[18] Green, I., and Etsion, I., 1986, "Pressure and Squeeze Effects on the Dynamic Characteristics of Elastomer O-Rings Under Small Reciprocating Motion," ASME J. Tribol., **108**(3), pp. 439–444.
[19] Green, I., and Casey, C., 2005, "Crack Detection in a Rotor Dynamic System by Vibration Monitoring—Part I: Analysis," ASME J. Eng. Gas Turbines Power, **127**(2), pp. 425–436.
[20] Varney, P., and Green, I., 2012, "Crack Detection in a Rotor Dynamic System by Vibration Monitoring—Part II: Extended Analysis and Experimental Results," ASME J. Eng. Gas Turbines Power, **134**(11), p. 112501.
[21] Etsion, I., 1982, "Dynamic Analysis of Noncontacting Face Seals," ASME J. Tribol., **104**(4), pp. 460–468.
[22] Etsion, I., 1980, "Squeeze Effects in Radial Face Seals," ASME J. Lubr. Technol., **102**(2), pp. 145–151.
[23] Etsion, I., and Sharoni, A., 1980, "Performance of End-Face Seals With Diametral Tilt and Coning—Hydrostatic Effects," ASLE Trans., **23**(3), pp. 279–288.
[24] Sharoni, A., and Etsion, I., 1981, "Performance of End-Face Seals With Diametral Tilt and Coning—Hydrodynamic Effects," ASLE Trans., **24**(1), pp. 61–70.
[25] Green, I., 1987, "The Rotor Dynamic Coefficients of Coned-Face Mechanical Seals With Inward or Outward Flow," ASME J. Tribol., **109**(1), pp. 129–135.
[26] Green, I., 1989, "Gyroscopic and Support Effects on the Steady-State Response of a Noncontacting Flexibly Mounted Rotor Mechanical Face Seal," ASME J. Tribol., **111**(2), pp. 200–208.
[27] Green, I., and Etsion, I., 1986, "A Kinematic Model for Mechanical Seals With Antirotation Locks or Positive Drive Devices," ASME J. Tribol., **108**(1), pp. 42–45.